
EFDA–JET–PR(03)23

V Riccardo and JET EFDA contributors

Disruptions and Disruption Mitigation

Disruptions and Disruption Mitigation

V Riccardo and JET EFDA contributors*

EURATOM/UKAEA Fusion Association, Culham Science Centre, Abingdon, OX14 3DB, UK

** See annex of J. Pamela et al, "Overview of Recent JET Results and Future Perspectives",
Fusion Energy 2000 (Proc. 18th Int. Conf. Sorrento, 2000), IAEA, Vienna (2001).*

Preprint of Paper to be submitted for publication in
Plasma Physics and Controlled Fusion

“This document is intended for publication in the open literature. It is made available on the understanding that it may not be further circulated and extracts or references may not be published prior to publication of the original when applicable, or without the consent of the Publications Officer, EFDA, Culham Science Centre, Abingdon, Oxon, OX14 3DB, UK.”

“Enquiries about Copyright and reproduction should be addressed to the Publications Officer, EFDA, Culham Science Centre, Abingdon, Oxon, OX14 3DB, UK.”

ABSTRACT.

Detailed disruption related studies have been undertaken at JET in 2001-3 and are compared and contrasted with results from other tokamaks. An enhanced halo current detection system has allowed more precise asymmetry measurements to be made, confirming the assumptions in the ITER design guidelines. The runaway electron database has been systematically analysed and self-consistent simulations are underway. Disruption heat deposition, which is of fundamental importance for ITER, has been investigated in JET. It has been found that normally only a small fraction of the thermal energy goes to the divertor and that during the thermal quench some energy goes to the outer wall. The neutral point has been experimentally found and a plasma control model has been used to reproduce the dedicated discharges. Helium, neon and argon puffs have been applied as disruption mitigation techniques in JET following the success of recent studies in ASDEX Upgrade, TEXTOR and DIII-D.

1. INTRODUCTION

Plasma disruption is a sudden loss of magnetic confinement. The energy stored in the plasma is promptly released to the surrounding structures. Large toroidal loop voltage can accelerate runaway electrons, which may be lost to the vessel walls causing metallic components to melt. Elongated plasma configurations can lose vertical stability; if this occurs at nearly pre-disruption plasma current and thermal energy, it is called Vertical Displacement Event (VDE). When the plasma loses its equilibrium vertical position, it can contact the wall and part of its current (known as a halo current) can flow into the wall. The likelihood of having a VDE (large plasma vertical displacement and halo current) depends on the causes of the disruption and varies from device to device. Disruptions are likely to be unavoidable, at least on an occasional basis, in the operation of a tokamak. A better understanding of disruption loads is important, as they have a strong influence on the design of any new tokamak device [1].

The average poloidal halo current contributes to the vertical force on the vessel at the disruption, while the local halo current density is a determinant in the design of in-vessel components. The design halo current density can be extrapolated from the product of the halo fraction (f , ratio of the toroidally averaged poloidal halo current and the pre-disruption plasma current) and the degree of asymmetry, represented by the Toroidal Peaking Factor (TPF, ratio of the maximum to the average poloidal halo current). In the 2001 shutdown the JET halo current diagnostics have been refurbished [2] allowing for more reliable measurements of the poloidal halo current in a larger number of toroidal locations. This has led to a better estimate of the halo fraction and TPF. The analysis of recently collected data is compared with those of MAST and ASDEX Upgrade in section 2.

Runaway Electrons (REs) have systematically been produced in low elongation, limiter plasmas disrupted with impurity puffs. The ARENA code [3] has been used to self-consistently model the electron kinetics in one of these shots. Section 3 includes this numerical study and the discussion of the database.

Disruption heat loads are reported in section 4 and disruption mitigation results in section 5. As part of the disruption mitigation studies, the existence of the neutral point (the plasma centroid position at which the plasma vertical displacement at the disruption is minimised) has been established experimentally and reproduced using the CREATE_L linearized plasma response model [4]. Fast puffing of helium and higher-Z gases (neon and argon) was used to ameliorate disruptions: reduce poloidal halo currents and divertor heat loads, avoid the RE generation. Due to limitations of the present JET gas injection system only halo currents could be reduced.

2. HALO CURRENT

A current flowing in the outer region of the plasma and having a part of its path in the vessel wall is called a halo current. While in the plasma part of its path, the halo current follows the magnetic field lines (under a force-free assumption), once in the conductive structures it is free to choose the easiest path. The halo current is driven by the toroidal voltage induced by the core current decay and by the poloidal voltage due to the change in enclosed toroidal field, and it is also fed by plasma motion convecting core current into the halo [5]. The dominant source depends on the characteristics of each machine: highly vertically unstable plasmas can have very fast disruptions with high halo currents, while more vertically stable plasmas have fast events decoupled from large displacement events.

A good understanding of halo current requires reliable measurements. The technique employed in JET is to estimate the poloidal halo current from the variation of toroidal field within the halo current path outside the plasma. Originally JET had two toroidal field pick-up coils at the top, and at the bottom, of the vessel in two locations set 180° apart, and some local halo current density probes [6]. Only one of these toroidal field pick-up coils is still working, therefore, during the 2001 shutdown three Rogowski coils and three toroidal field pick-up coils have been installed together with the Improved Upper Inner Wall Protection (IUIWP).

While with the two original measurement stations at 180° the TPF for a $n=1$ mode could be underestimated by 50%, with three at 90° it can only be underestimated only by 25%. The phase where the saturated kink mode locks during disruptions is not fixed, therefore over a large number of events the worst TPF is captured. This is confirmed by Fig.1 which shows that the TPF measured by the IUIWP toroidal field pick-up coil in recent disruptions is not larger than it used to be with only two probes. Figure 1 also contains the ITER reference design data for halo current [1]; the JET data are characterised by lower TPF than most of other machines. The typical design value of the product TPF times halo fraction, $TPF \cdot f$, for ITER is 0.5, while 0.75 is the extreme value. Figure 2 shows that for JET disruptions $TPF \cdot f$ is generally less than 0.5; the only event with $TPF \cdot f$ above 0.5 is a high-triangularity high-elongation deliberately triggered (by offsetting the radial field) VDE at low- q ($q_{95} < 2.5$). Figure 2 also shows that $TPF \cdot f$ does not depend on the plasma current, it depends instead on the plasma current quench rate: the largest $TPF \cdot f$ occurs when the 95-35% plasma current quench rate is slow (< 100 MA/s). Only at this low plasma current quench rate the q_{\min} , the minimum value reached by the cylindrical approximation safety factor during the disruption, decreases to values less than 1.5.

All the events with TPF·f larger than 0.2 have a $q_{\min} < 1.5$. No trend in the poloidal halo current fraction or in the TPF has been found in a set of disruptions triggered (by offsetting the radial field) at constant plasma current and configuration but different boundary safety factor, q_{95} . In fact, the I_p/q_{95} scaling proposed for the poloidal halo current data in Alcator C-Mod [7, 8] and supported by COMPASS-D data [9] does not fit JET, nor DIII-D data [10], where large variations of poloidal halo current are observed at fixed I_p/q_{95} . The main cause for a deviation from the I_p/q_{95} scaling is the influence of the pre-disruption thermal content on the current decay rate [11]: high- β_p disruptions are faster, maintain a higher safety factor and have less poloidal halo current. This is typical of JET and DIII-D, but cannot be representative of devices with very vertically unstable plasmas, which may produce disruptions with extremely rapid current decays, as well as high halo currents [5].

The ASDEX Upgrade bottom divertor is equipped with 90 shunts distributed in poloidal and toroidal arrays. Such a good distribution allows the measurement of very local asymmetries and the observation of the halo current footprint on the divertor. The halo fraction in ASDEX Upgrade can be as large as 50%, and it scales with the amplitude of the plasma vertical displacement during the disruption, similarly to what is observed at JET. Like in JET the halo TPF of ASDEX Upgrade disruptions is larger when the cylindrical safety factor reaches low values. However, while in JET the cylindrical approximation boundary safety factor (q_{cyl}) has to decrease to ~ 1 in order to have large asymmetries, a $q_{\text{cyl}} \sim 2$ triggers halo asymmetries in ASDEX Upgrade.

In ASDEX Upgrade, high q_{95} density limit disruptions and VDEs typically generate asymmetries in the halo current. In disruptions with strong MHD activity, hardly any asymmetry has been observed, suggesting that the MHD activity prevents the plasma from re-heating and developing a configuration that could lead to a kink mode [12]. In shots where a kink mode would be expected, this can be suppressed by the injection of a killer pellet (see section 5.3), as reported also for DIII-D [13].

Over 150 individual halo detectors are fitted in MAST [14]. All the current sources and sinks have been identified. Generally, in downward events, most of the halo current is collected at the bottom of the centre column (70-80%) and on the inner target (20-30%) and leaves the vessel at the screen of the outer poloidal field coil and at the rib limiters.

MAST halo current data have been compared to the ITER database (Fig.1) as in [14]. The maximum halo current fractions are similar to those observed in conventional aspect ratio tokamaks. However, under normal spherical tokamak operations, with plasma current above 350kA, halo current fractions above 25% have not been observed. Large halo current fractions are seen at low plasma currents, usually associated with large aspect ratio, and fractions up to 85% have been produced in experiments where the plasma was driven highly unstable by ramping down the poloidal field currents. Comparison of the peaking factor at four poloidal positions shows a general trend for the TPF to be higher outboard. This can be partly explained in terms of the increased differences in poloidal to toroidal path lengths at larger radius (i.e. toroidal path shorts out the asymmetry). Measurements carried out during the MAST divertor biasing experiment [14] suggest that during VDEs, the plasma acts more as a voltage

source than a current source when generating halo currents. Therefore by altering the resistance of the current path it is possible to limit these currents.

3. RUNAWAY ELECTRONS

Depending on the electron temperature and density, runaway electrons can be generated by the loop voltage of a disruption. The runaway beam can become dangerous when it interacts with the in-vessel components and the vessel walls (causing melting of metals). A good understanding of the RE phenomenology will improve the chances of coping with (or avoiding) runaway electrons in operation at high plasma current, where they are most likely.

In the original survey of JET shots with RE production [15] the variations in behaviour caused by different configurations (including carbon and beryllium limiters) were identified, and subsequently analysed [16, 17]. After the installation of the divertor, rather few discharges had long lasting runaway electrons and this is attributed to the more vertically unstable plasma columns caused by the non-symmetric configuration [18].

A recent and more detailed examination of the hard X-ray emission following disruptions showed that many discharges had some spontaneous runaways even though the characteristic plasma current plateau did not develop. In the following the integral of the neutron emission rate measured via the fast sampled ^{235}U fission chamber current [19] during the disruption is taken as a measure of the number of runaway electrons with energy $>10\text{MeV}$ which produced (γ,n) neutrons after leaving the RE beam and referred in the following as the number of photoneutrons. In Fig.3, a survey of a large number discharges shows that REs occur after a disruption when the value of B_t exceeded the threshold of 2T, similar to JT-60U [20] and TS [21]. The JET data show no clear threshold on the value of the boundary safety factor (q_{eff}). This is instead present in the JT-60U data [20], where no RE are observed for $q_{\text{eff}} < 2.5$ at the disruption. In addition, the number of photoneutrons increases by two orders of magnitude as the toroidal field goes from 2T to 3.5T; a similar enhancement in the strength of the RE population has been observed in FTU [22]. Analysis of a number of disruptions with runaway electrons shows that the number of photoneutrons has an upper limit, which scales with the initial plasma current decay rate. Although the chances of surviving (large number of photoneutrons) are better at low elongation, no trend in RE generation has been found with the elongation (i.e. an initial burst of RE can be observed at any elongation).

A systematic plasma current scan at $B_t = 3\text{T}$ and 3.4T on low elongation (limiter) deliberate (argon puffing) disruptions has been conducted to further the understanding of RE production and to try to develop control scenarios (see section 5.2). At both fields the generation is maximum at $\sim 2\text{MA}$ and drops to almost zero at higher and lower currents. It is thought that runaway beam generation does not occur at low plasma currents as the electric field is too low; while at high currents, magnetic fluctuations may prevent their formation [23]. Fig. 4 shows one of these dedicated discharges, Pulse No: 53786, which produced a very long-lasting RE beam. Diffusion losses at these toroidal field and plasma current (3T and 2MA) do not seem to play a significant role in the removal of electrons from the RE

beam. In fact, once the plateau is reached the current is kept constant, until the beam crashes into the vessel wall, as indicated by the bursts in the neutron and γ -rays measurements. There are delays between the loop voltage peak and the observation of γ -rays and of neutrons. In fact, when there is an appreciable number of runaway electrons with an energy of $\sim 1\text{MeV}$, γ -rays will be observed; whereas neutron production requires the (γ, n) threshold of $\sim 10\text{MeV}$ to be exceeded.

Pulse No: 53786 has been analysed with a 0D model [23] and subsequently with the ARENA code [3], which solves the relativistic drift kinetic equation for electrons in toroidal geometry. Crucially, both primary (Dreicer) and secondary (avalanche, [24, 25]) runaway production are taken into account, and the evolution of the toroidal electric field is calculated self-consistently in ARENA. The current carried by the runaways thus modifies the electric field responsible for the runaway production in the first place, making the dynamics non-linear. Background plasma parameters such as electron density and temperature are specified as input parameters to the code, and the thermal quench is modelled by letting the electron temperature fall in a prescribed way. This causes the resistivity to increase and the inductive toroidal electric field to rise, triggering runaway generation: first by primary generation and later by the avalanche mechanism [24, 25]. This limits the further growth of the electric field and eventually brings it down to values where no more runaways are generated.

Figure 5 shows an example of such a simulation with parameters chosen to match JET discharge 53786. The density profile was taken to be $n_e = [1 - 0.9 (r/b)^2]^{1/2} \times 5 \cdot 10^{19} \text{ m}^{-3}$, the pre- and post-disruption temperatures were $(T_0, T_1) = [1 - 0.9 (r/b)^2]^2 \times (1.4 \text{ keV}, 20 \text{ eV})$, where $b = 1\text{m}$ is the radius of the plasma-vacuum interface, and the time scale for the thermal quench was $t_0 = 1\text{ms}$. There is good agreement between the computed electric field and the measured (at $\sim 1.8\text{m}$ radius) toroidal voltage (Fig.4). The runaway production commencing 4ms after the onset of the thermal quench is initially very fast and due to primary generation. This triggers a secondary avalanche, which lasts for about 5ms. As predicted by theory [24, 25], most runaways are generated by the avalanche mechanism (when a RE knocks another electron into a runaway status), and the process is quite sensitive to the electron density. At higher post-disruption densities, runaway production is slower and less effective, so that a smaller fraction of the current is carried by runaways.

The runaway electrons energy spectrum consists of two parts: a drawn-out tail and a high-energy “bump”. The bump is mainly made up of primary (Dreicer) runaway electrons, while the tail represents secondary (avalanche) electrons. The Dreicer runaway electrons are produced first and are therefore accelerated longest and reach the highest energy, while the avalanche electrons have lower energy. The energy of the Dreicer runaway electrons is consistent with the flux change available for their acceleration [26]: $\sim 1\text{Vs}$ at the plasma axis gives $\sim 15\text{MeV}$.

The code can also be run with radial diffusion (caused by magnetic fluctuations) acting on the runaways, which tends to suppress avalanche runaway production [27]. With a diffusion coefficient equal to the Rechester-Rosenbluth value [28], a significant effect is observed if the magnetic fluctuation level exceeds $\delta B_t/B \sim 10^{-4}$, just above the upper end (5×10^{-5}) measured in the fixed- B_t current scan experiments [23].

4. HEAT LOADS

Disruption heat loads are crucial to the survival of the divertor of any next generation machine. If, as currently included in the ITER design criteria, all the thermal energy of the plasma is deposited on the divertor on a limited area (only three times the steady state area), the range of suitable divertor materials becomes very limited.

In most of the JET disruptions the sum of the radiated energy (which includes also the divertor) and the energy deposited on the divertor tiles is less than the pre-disruption energy. The energy not found in these sinks can be exchanged with the poloidal field coils and the passive structures or conducted elsewhere in the vessel.

A detailed description of the diagnostics used to measure the heat fluxes in JET disruptions can be found in [29], which also includes a detailed analysis of limiter density limit disruptions. Here it is only recalled that this type of disruption tends to produce runaway electrons and that when this happens the heat loads, as seen by the Thermocouple (TCs) can be toroidally non-uniform. Density limited or collapsed Internal Transport Barriers (ITBs) discharges are the only other disruption type systematically prone to RE generation, since their loop voltage is higher (the current quench is faster).

Figure 6 shows that the power footprint on the divertor at the disruptive end of pulse 58009 is very similar to the previous Edge Localised Modes (ELMs) in terms of location, width and peak power density. However, the power deposition lasts longer than in an ELM (hence a larger deposited energy), as it covers both the H-L transition and the disruption. Before the H-L transition the plasma thermal energy was ~ 5 MJ and the magnetic energy ~ 18 MJ. During the H-L transition and the disruption the infra-red (IR) data shows that ~ 5 MJ are deposited on the divertor (but only 1MJ during the 20ms long thermal quench) and the bolometry shows that ~ 16 MJ are radiated. This event, including the H-L transition, is representative of the many JET H-mode disruptions as far as the divertor heat loads are concerned.

In the locked mode disruption of Fig.7 over two thirds of the thermal energy are lost in ~ 300 ms before the major disruption: from 3.6MJ to 1.0MJ, while ~ 1 MJ is still injected by the neutral beams. This slow energy loss is associated to the presence of MHD activity. This typically occurs in low- q operation or following an increase of edge impurity, both lead to an unstable current profile with the $q=2$ surface just outside a steeper than normal current gradient, which is unstable to tearing modes. During the whole event the energy deposited on the divertor is ~ 3.5 MJ, of which ~ 1 MJ is lost at the concluding disruption: a close match to the thermal energy lost by the plasma. The power footprint is wider at the disruption than during the locked mode, and already the locked mode footprint is wider than the equilibrium one.

ITB collapse discharges are associated with a fast growing, rotating, disruptive, $m=2 / n=1$ kink mode. The $n=1$ mode can be observed with Mirnov probes [30] and the poloidal structure with electron temperature measurements. The electron temperature measurements also show non-linear ballooning modes superimposed on the outer kink, similar to observations in TFTR [31]. The ballooning mode pushes a segment of a central field line out into the outer plasma, ejecting hot plasma into the scrape

off layer or onto the walls. In some ITB collapse disruptions, Langmuir probes, both at the divertor and on the outer poloidal limiter, register an interaction during thermal quench. Although the data in Fig. 8 is not quantitative, the divertor signal is similar to that seen during ELMs, while the limiter signal is not saturated during ELMs. This indicates that the X-point is not lost at the thermal quench and that substantial interaction on the outer poloidal limiter is taking place. Fig. 8 also has a non-calibrated fast-sampled disruption radiation energy waveform, which shows that radiation starts slowly at the thermal quench and that a significant amount of energy is lost through this channel only during the current quench.

Similar to the JET disruptions, also the ASDEX Upgrade disruption have a divertor power footprint larger than three times the equilibrium power footprint [32]. Differently from JET, both ASDEX Upgrade [32] and DIII-D [33] can have the equivalent to the whole thermal energy deposited on the divertor during the disruption.

5. DISRUPTION MITIGATION

The aims of disruption mitigation are:

- to reduce the amount of energy conducted to the divertor;
- to reduce poloidal halo currents, and related vessel stresses and in-vessel components electromechanical loads;
- to increase the background density so that RE production is prevented.

Halo currents and vessel forces are reduced by operating near the neutral point. In addition, working near the neutral point gives a longer intervention time to activate disruption amelioration techniques (in particular to avoid runaway electrons). Full exploitation of disruption mitigation will be greatly assisted if neural networks, able to reliably predict the approach of a disruption, are developed. Neural networks are systems able to recognise a forthcoming plasma disruption within a time sufficient to carry out ameliorating actions. Since disruptions can occur in different regions of the operating space and depending on the mode of operation have different precursors, statistical data analysis and the experience gathered over several years of operation are used to train neural networks. Off-line testing of the network on a large number of discharges is necessary to attest its reliability. Neural networks have already been routinely employed to trigger killer pellets [34] and could be used for high pressure gas jets too, as long as the prediction is available early enough for the mitigation technique to be effectively applied.

5.1 NEUTRAL POINT EXPERIMENTS

Fast axisymmetric plasma disturbances create an imbalance of forces between external currents and the plasma, which can cause the plasma to move vertically in a preferential direction (i.e. upward or downward). There is a position for the plasma current centroid where ideally this imbalance is zero. When a given perturbation at a given instant t_0 excites the (axisymmetric) unstable vertical mode with an initial vertical displacement δz_0 , the plasma vertical displacement δz evolves exponentially as

$\delta z = \delta z_0 e^{\gamma(t-t_0)}$, where γ is the growth rate of the vertical instability. Assuming the quantity δz_0 is a function of the initial plasma centroid vertical position where the instability is excited, which changes sign, the neutral point (NP) is the vertical position at which δz_0 vanishes.

Some dedicated experiments performed on JET, and related simulations, demonstrate the existence of a neutral point for density limit disruptions of a plasma, specially designed to be set at different vertical equilibrium positions without altering the shape. The plasma moves upwards (downwards) when the disruption is triggered with the plasma below (above) the NP. The CREATE_L linearized plasma response model [4] applied to such configurations is able to predict and explain the most significant qualitative features of the experiment [35]. This provides a valuable validation of the CREATE_L code.

The growth rate does not significantly vary among the configurations analysed. Therefore, the location of the neutral point is determined by plotting, Fig. 9, the vertical displacement (dz_p) of the plasma current centroid after a given time interval (3 ms) from the thermal quench (H_α spike), as a function of the initial plasma vertical position. The quantity dz_p depends almost linearly on the initial vertical plasma position, and changes sign around ≈ 20 cm. The directionality is opposite to the intuitive one. The directionality of ASDEX Upgrade disruptions [36] deviates from intuitive forecasts, but this deviation can be explained taking into account the dynamics of the current profile. In ASDEX Upgrade a large number of bottom divertor configurations positioned well above the neutral point computed via TSC [37] move downward at the disruption, while some go upwards. TSC simulations show that the slower is the drop in internal inductance, the weaker is the drag towards the X-point, so that the actual neutral point is at a higher position. The dependence on the internal inductance is a reflection of the fact that the neutral point, analytically, is a function of the plasma magnetic configuration and of the disturbance leading to the plasma disruption.

5.2 HIGH PRESSURE GAS PUFFING IN JET

Only two gas injection valves can operate at relatively high pressure (2.5 bar) and on short time scales at JET. The maximum amount of injected impurity particles in < 50 ms is $\sim 9 \cdot 10^{21}$. Three gases have been employed: helium, neon and argon. None of these had an adverse effect on the breakdown of the following discharges. The amount of injected helium had to be limited in order to avoid spontaneous regeneration of the divertor cryopump (the neutral beam boxes had to be closed for the same reason).

Helium alone has been successfully used to prevent RE formation [29] by pre-emptive puffing during impurity induced limiter plasma density limit disruptions at favourable toroidal field and plasma current (3T and 2MA). The helium puff prevented RE generation for at least two reasons: the background density was higher and the plasma current decay was slower.

In deliberate (offset of the radial field) VDEs, the main effect of (feed-forward) helium injection was to slow down the disruption, leading to overall more demanding electromagnetic loads (e.g. vessel forces [29]), as explained in section 2. Instead, feed-forward puffing of neon or argon is sufficient to at least transform a potential VDE into a density limit disruption and significantly reduce the

electromechanical loads as shown in Fig. 10. When a high-Z gas is used, there is hardly any correlation between electromechanical loads on the vessel and the gas used (or its reservoir pressure); the loads only depend on the delay between the thermal quench and the loss of vertical equilibrium position. On the other hand the effect on the electron temperature of neon and argon, as puffed into these discharges, is rather different. While the drop in electron temperature is much faster than in a “normal” disruption when neon is puffed; there is no significant change in the electron temperature dynamics when argon is puffed. The argon-puffed thermal quench is better explained as a slow radiative collapse instigated from the highly radiating edge plasma that eventually just shrinks the current profile to an unstable position. It is unclear how much argon is actually available to the central plasma, as the gas beam could have degraded after injection: both the argon and the neon gas puffs take at least 20ms before becoming effective at the plasma centre. This is equivalent to an average speed of 75m/s, less than half the sonic speed of argon or neon. Simulations have been carried out using KPRAD [38] to find effective gas parameters that match measured disruption times in a triggered VDE with a neon gas puff. The plasma thermal quench occurs ~23 ms after the initiation of the neon gas puff. The current quench decay time is ~6 ms. The neon is provided at low pressure, so it is promptly ionised in the plasma edge and pinch/diffuse into the central plasma on a time scale set by the injection rate and the cross-field plasma transport. In the KPRAD simulation, the neon is assumed uniformly distributed through the plasma. A constant neon injection rate into the plasma is assumed over 50 ms. In the attempt to simulate the effects of edge screening, the injection rate and the initial charge state of neon are scanned. The thermal quench time can be obtained by reducing the injection rate to a fifth of the experimental value. At this injection rate, experimental results are consistent with an initial charge state of ~7, representative of a situation dominated by plasma transport of the neon. Therefore, KPRAD modelling suggests that the JET neon gas puff does not penetrate effectively as a neutral. Although the JET gas puff experiments have not been successful (argon and neon did not penetrate effectively), these experiments should be repeated, if a suitable injection valve becomes available, so as to produce conditions closer to those in DIII-D and enable size extrapolation towards ITER. Assuming that the parallel field is not affected by the amount of injected impurity, as shown in [33], to ensure RE prevention the total electron density (that is bound and free electrons) needed to increase the critical field ($E_c = mcv/e \sim 10^{21} n_{e,tot}$) as to match the computed parallel field of 10 V/m (Fig.5) is $\sim 10^{22} \text{ m}^{-3}$, equivalent to $\sim 8 \cdot 10^{22}$ neon atoms. This value is similar to the one required in DIII-D and ITER [33], and ten times larger than the one presently achievable at JET ($8 \cdot 10^{21}$).

5.3 DISRUPTION MITIGATION IN DIII-D, TEXTOR AND ASDEX UPGRADE

In DIII-D recent disruption mitigation experiments [33] saw the reduction (or elimination) of thermal loading of the divertor surfaces, of poloidal halo currents and of runaway electrons generation. High-pressure jets of neon and argon reach the centre of the plasma as neutral gases at sonic velocity. The fast valve, fitted on a 70 bar reservoir, releases $\sim 4 \cdot 10^{22}$ particles in 2-5ms, achieving an impurity density ~ 35 times larger than the typical electron density ($3 \cdot 10^{19} \text{ m}^{-3}$). When the target is a stable

plasma, no significant MHD activity is observed until a large amount of radiation comes from the core, where the impurity has been deposited. The electron temperature drops in ~ 0.2 ms and the plasma current decay starts promptly. More than 95% of the plasma stored energy is radiated. The gas injection has no adverse effect on any pumping system and there are no breakdown problems for the following discharge. The plasma control system has been programmed to inject neon when a VDE is detected in discharges where the event is deliberately initiated by disabling the vertical control system. In these events the energy deposited on the divertor is reduced by a factor of 2 for the inner target and a factor of 5 for the outer target with respect to non-mitigated events. Also the poloidal halo currents are reduced, because the plasma current decays more rapidly than the plasma movement into the wall, so keeping the boundary safety factor higher than in non-mitigated disruptions.

Differently from the use of killer pellets (frozen impurity pellets injected in the plasma at high speed) [10, 13], no significant population of runaway electrons has been observed after killer jets in DIII-D. Both techniques cause rapid radiative cooling and current quench, but the gas jet injects ~ 100 times the number of atoms (although the number of free electrons is only moderately higher). A fast valve has been developed in TEXTOR [39] in order to prove runaway suppression by fast helium puffing. This was tested in low density runaway discharges. The runaway electrons start interacting with the injected helium within 0.5ms of the opening of the valve and are quickly slowed down. The hard X-ray detectors show that the runaway electrons are not expelled to the wall at their original (high) energy, therefore they must lose most of their energy interacting with the injected helium.

A fast valve similar to the one used in TEXTOR has been developed for ASDEX Upgrade [40] and used in a set of feed-forward disruption mitigation experiments carried out using helium, neon and argon [41]. The measured current quench rate of limiter plasmas goes from ~ 20 MA/s with helium to 60-80MA/s with neon and argon; the delay between the gas reaching the plasma edge and provoking the disruption was 12ms for helium, 4ms for neon and 2ms for argon. Argon caused some contamination, while helium was inefficient. Runaway electrons were observed in a few discharges with density lower than $4 \cdot 10^{19} \text{ m}^{-3}$ and toroidal field higher than 2 T. Similarly neon pellets [42], in early mitigation experiments, although effective with respect to heat and electromechanical loads, were later found to give rise to runaway electrons. In contrast silicon or titanium powder in molten polyethylene killer pellets [34] did not give rise to long-lived runaway electrons and were able to eliminate the energy deposited on the divertor at the thermal quench and half the poloidal halo current. The experience described in [34] is one of the few examples of usage of a feed-back activation of the mitigation technique (based on a neural network, while usually experiments are carried out in feed-forward).

CONCLUDING REMARKS

Data from the improved halo current measurement system confirmed the previous JET results on halo current and toroidal peaking factors. This is consistent with having less demanding halo current design criteria coming from large machines and confirms the ITER assumptions.

In JET, like in JT-60U and TS, there is a toroidal field threshold below which disruption runaway electrons are not observed. In addition, it has been shown that the RE beams are stronger at higher toroidal fields. Modelling of a JET discharge with sustained runaway electron beam shows that most of the runaway current is carried by avalanche electrons, in agreement with the ITER predictions.

In JET, the sum of divertor deposited energy and radiated energy is not sufficient to account for the total (thermal plus magnetic) pre-disruption plasma stored energy. The missing energy can be exchanged with the poloidal field coils and the passive structures [29] or conducted elsewhere in the vessel, and in fact at the outer poloidal limiter, as well as at the divertor, Langmuir probes can register current spikes during the thermal quench. In H-mode disruptions the peak divertor power density is similar to that of preceding ELMs but the power pulse may last longer. Typically only a small fraction of the plasma thermal energy is deposited on the divertor. When the energy deposited on the divertor is a large fraction of the plasma thermal energy, the footprint is wider than in normal operation.

Disruption mitigation can be achieved with mixtures of techniques. Operation at the neutral point, which alone already significantly reduces halo current loads, is helpful if fast gas jets have to be employed to ameliorate runaway electrons, as a longer intervention time is available since the vertical position is lost more slowly. Killer pellets are suitable for routine operation in conjunction with a neural network [34] and are efficient in reducing the electro-mechanical forces and the energy deposited on the divertor, but they tend to produce runaway electrons. To avoid RE generation the density needs to be increased, that implies the number of injected particles has to be large. This can be achieved with high pressure gas jets, which have been successfully tested in DIII-D and to lower specification in ASDEX Upgrade and JT-60U.

Recent JET data confirms the ITER design guidelines for halo currents. The ITER divertor disruption heat loads assumptions may be too conservative. As at JET some energy is deposited in the main chamber, this disruption heat load sink should be further investigated, as should differences with the results on ASDEX Upgrade and DIII-D. Disruption mitigation techniques applicable to ITER have been successfully tested in DIII-D, ASDEX Upgrade and JET.

ACKNOWLEDGEMENTS

Work performed under EFDA and partly funded by EURATOM and the UK Engineering and Physical Sciences Research Council. The disruption heat load analysis has been co-ordinated by the Disruption Working Group of the European Plasma Wall Interaction Task Force. Thanks to Gabriella Pautasso, James Paley and Fredrik Andersson, who are not included in the JET EFDA contributors.

REFERENCES

- [1]. ITER Physics Basis 1999 Nucl. Fusion 39 Chapter 3 Section 4
- [2]. V Riccardo et al., Refurbishment of the JET halo current diagnostics, accepted for publication in Fusion Engineering and Design

- [3]. LG Eriksson, P Helander, Simulation of runaway electrons during tokamak disruption, for publication in Computer Physics Comm.
- [4]. R Albanese, F Villone, Nuclear Fusion **38** (1998) 723
- [5]. DA Humphreys, AG Kellman, Physics of Plasmas **6** (1999) 2742
- [6]. P. Andrew et al., Proc. 17th IEEE/NPSS Symposium on Fusion Engineering (1997) 108
- [7]. Granetz et al., Nuclear Fusion **36** (1996) 545
- [8]. Granetz, Disruption halo currents with C-Mod's new divertor, APS-DPP, Orlando (2002)
- [9]. P Knighth et al., Nuclear Fusion **40** (2000) 325-337
- [10]. Kellman et al., in Fusion Energy 1996 (Proc. 16th Int. Conf. Montreal, 1996), Vol.1, Vienna (1997) 739
- [11]. V Riccardo, Fusion Science and Technology **43** (2003) 493
- [12]. G Pautasso et al., 28th European Physical Society Conference on Plasma Physics and Controlled Fusion, Madeira (2001) P-1.005
- [13]. TE Evans et al., Journal of Nuclear Materials 241-243 (1997) 606
- [14]. R Martin et al., 29th European Physical Society Conference on Plasma Physics and Controlled Fusion, Montreux (2002) P-1.053
- [15]. GR Harris, Comparisons of the Current Decay during Carbon-bounded and Beryllium-bounded Disruptions in JET, JET-R(90)07 (1990)
- [16]. J Wesson, RD Gill, M Hugon, FC Schiller et al., Nuclear Fusion **29** (1989) 641
- [17]. RD Gill, Nuclear Fusion **33** (1993) 1613
- [18]. RD Gill et al., Nuclear Fusion **40** (2000) 163
- [19]. ON Jarvis, Treatment of the KN1 data channels, JET-TN(87)04 (1987)
- [20]. R Yoshino et al., Nuclear Fusion **39** (1999) 151
- [21]. G Martin, Control of runaway electrons created during major disruptions, IAEA TCM on Avoidance and Control of Tokamak Disruptions, Culham, 1991
- [22]. FM Poli, B Esposito, G Maddaluno, Disruption generated runaways in FTU high field tokamak, 43rd American Physics Society Conference, Long Beach (2001) GP1.063
- [23]. RD Gill et al., Nuclear Fusion **42** (2002) 1039
- [24]. MN Rosenbluth and SV Putvinski, Nucl. Fusion **37** (1997) 1355
- [25]. P Helander, LG Eriksson and F Andersson, Plasma Phys. Control. Fusion **44** (2002) B 247
- [26]. O Jarvis et al., Nuclear Fusion **28** (1988) 1981
- [27]. P Helander, LG Eriksson and F Andersson, Phys. Plasmas **7** (2000) 4106
- [28]. AB Rechester and MN Rosenbluth, Phys. Rev. Lett. **40** (1978) 38
- [29]. V Riccardo et al., Plasma Physics and Controlled Fusion **44** (2002) 905
- [30]. GT Huysmans et al., Nuclear Fusion **39** (1999) 1489
- [31]. Fredrickson et al., Physics of Plasma **3** (1996) 2620
- [32]. G Pautasso, 30th European Physical Society Conference on Plasma Physics and Controlled Fusion, St Petersburg (2003) P-1.135

- [33]. DG Whyte et al., Disruption Mitigation using High-Pressure Noble Gas, Injection on DIII-D IAEA Conference, Lyon (2002)
- [34]. G Pautasso et al., Nuclear Fusion **42** (2002) 100
- [35]. F Villone, Neutral point detection in JET, accepted for publication in Fusion Engineering and Design
- [36]. Y. Nakamura et al., Plasma Phys. Control. Fusion, Vol **44** (2002) 1471
- [37]. SC Jardin et al., Journal of Computational Physics 66 (1986) 481
- [38]. DG Whyte et al., 24th European Conference on Controlled Fusion and Plasma Physics (1997) 21A, 1137
- [39]. KH Finken et al., Journal of Nuclear Materials **313-316** (2003) 1247
- [40]. A Savchikov, G Pautasso, KH Finken, G Mank, 29th European Physical Society Conference on Plasma Physics and Controlled Fusion, Montreux (2002) P-3.203
- [41]. G Pautasso et al., 29th European Physical Society Conference on Plasma Physics and Controlled Fusion, Montreux (2002) P-2.051
- [42]. G Pautasso, Nuclear Fusion **36** (1996) 1291

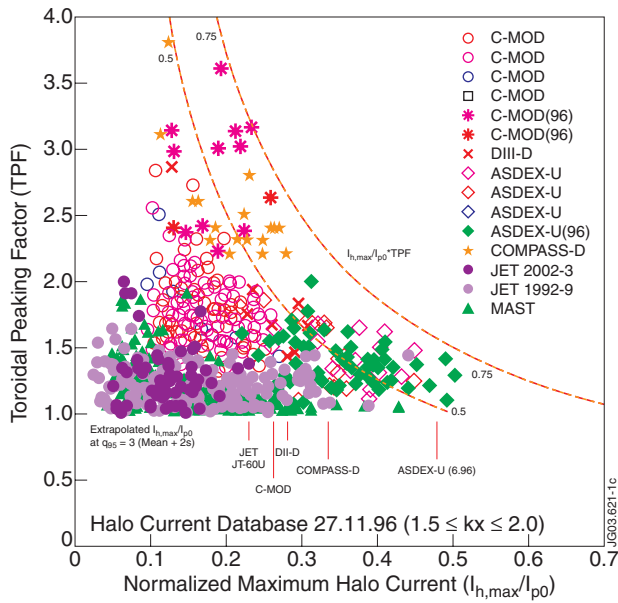


Figure 1: ITER halo current design data (from ref. [1], Fig.64 of Chapter 3) Overlaid with 1992-9 and 2002-3 JET and MAST halo data

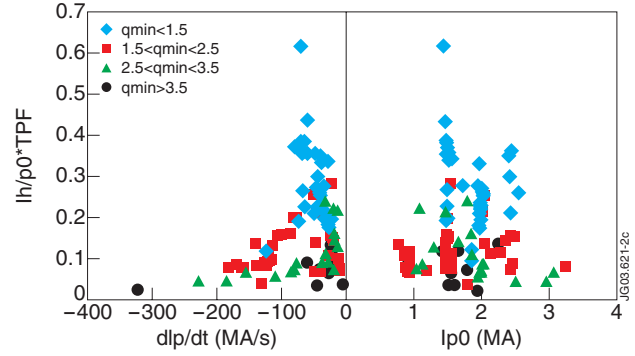


Figure 2: The product of halo fraction and TPF is plotted versus the plasma current quench rate (taken between 95% and 35% of the maximum plasma current) and the pre-disruption plasma current

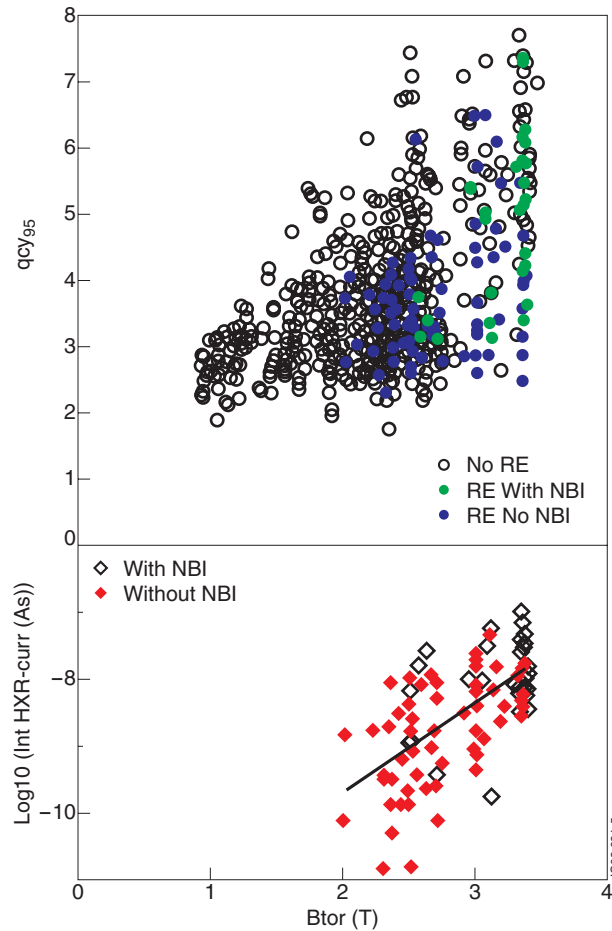


Figure 3: 1998-2003 JET disruption with RE (with and without NBI) are high lighted in the (B_p, q_{95}) -space among the other disruptions without RE; the number of photoneutrons increases on average by 2 orders of magnitude as the disruption toroidal field goes from 2T to 3.5T

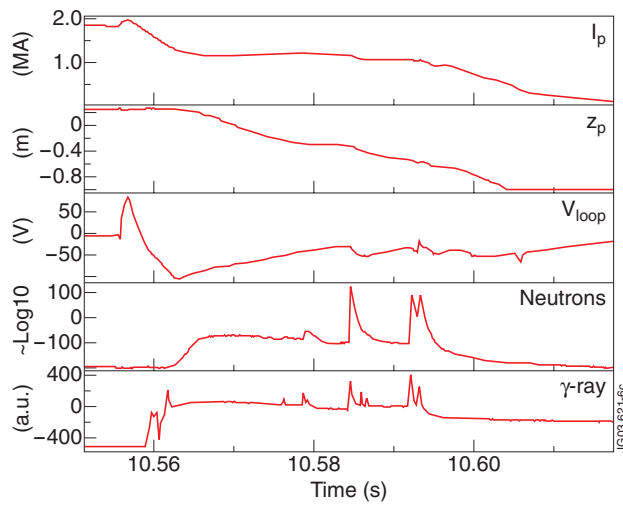


Figure 4: Time traces of plasma current and vertical position, loop voltage and the neutrons and γ -rays monitors for pulse 53786

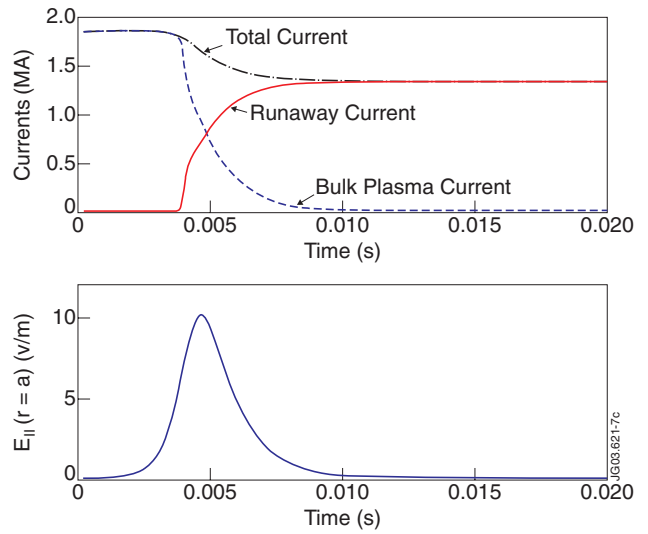


Figure 5: Evolution of the runaway and bulk plasma currents, and the electric field at the wall in an ARENA simulation of JET Pulse No: 53786.

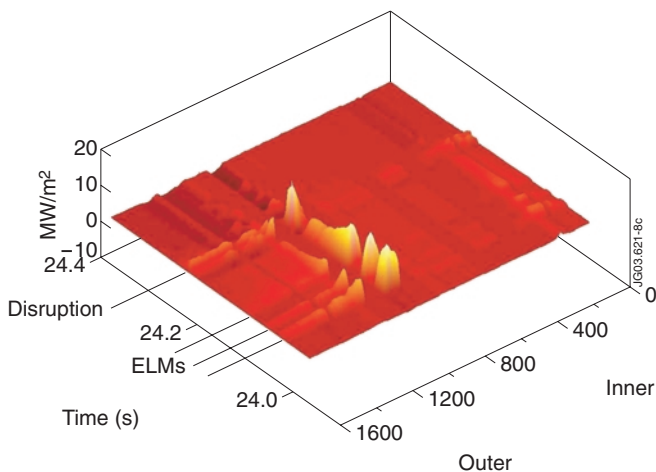


Figure 6: Power density on the divertor during an ELMY H-mode density limit disruption (JET Pulse No: 58009)

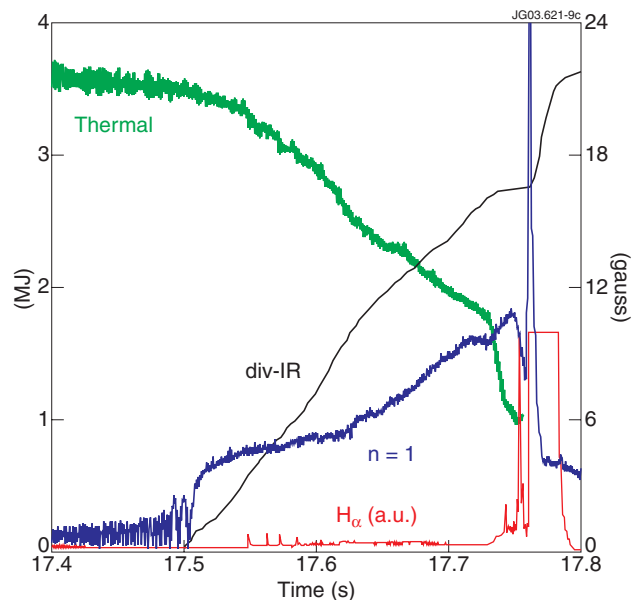


Figure 7: Time traces of the outer divertor H_α , the $n=1$ mode amplitude, the plasma thermal energy and the energy deposited on the divertor as measured by the IR camera (integral started when the mode locked) for Pulse No: 59027 (disruptive locked mode).

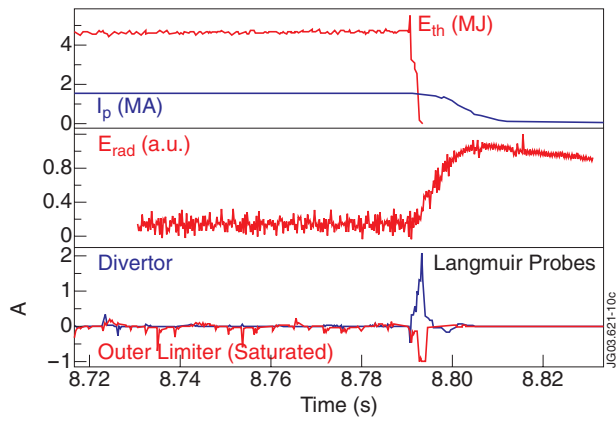


Figure 8: Plasma current, thermal energy, fast sampled radiated energy, poloidal limiter and divertor Langmuir probe currents for the ITB collapse of Pulse No: 58456

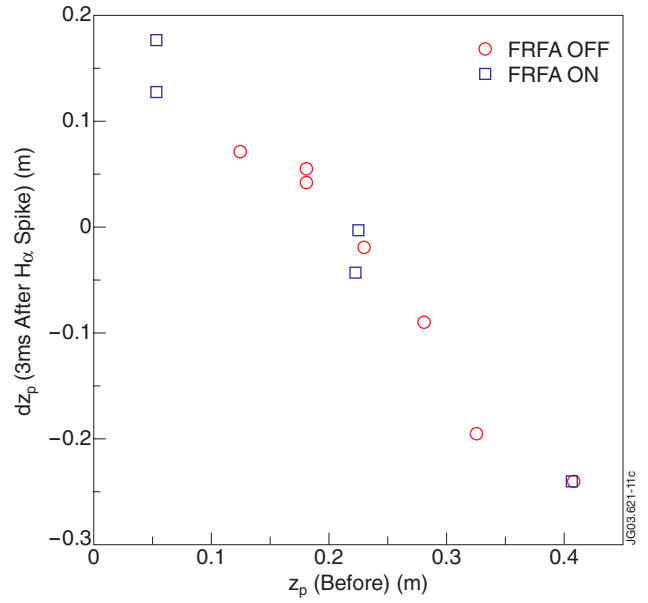


Figure 9: Vertical position displacement as a function of the starting vertical position

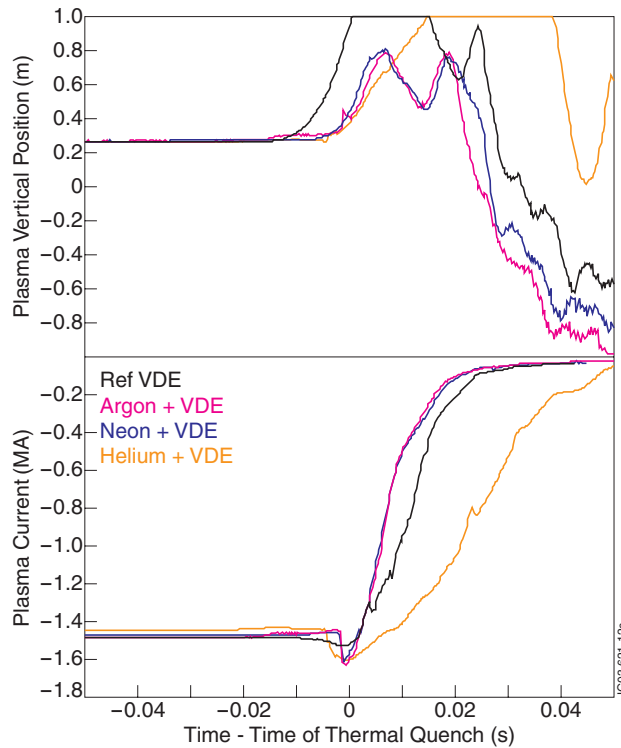


Figure 10: Plasma vertical position (top) and current (bottom) for a reference and three mitigated VDEs